## ORIGINAL RESEARCH

Blockade of Hepatocyte PCSK9 Ameliorates Hepatic Ischemia-Reperfusion Injury by Promoting Pink1-Parkin–Mediated Mitophagy

Yu Zhang,[1,2,3,*] Ziyi Wang,[1,2,3,*] Chenyang Jia,[4,*] Wenjie Yu,[1,2,3] Xiangdong Li,[1,2,3] Nan Xia,[1,2,3] Huiling Nie,[5] Likalamu Pascalia Wikana,[1,2,3] Minhao Chen,[1,2,3] Yong Ni,[4] Sheng Han,[1,2,3] and Liyong Pu[1,2,3]

[1]Hepatobiliary Center, The First Affiliated Hospital of Nanjing Medical University, Nanjing, China; [2]Key Laboratory of Liver Transplantation, Chinese Academy of Medical Sciences, Nanjing, China; [3]NHC Key Laboratory of Living Donor Liver Transplantation (Nanjing Medical University), Nanjing, China; [4]Department of Hepatopancreatobiliary Surgery, Shenzhen Second People's Hospital, The First Affiliated Hospital of Shenzhen University, Shenzhen, China; and [5]Affiliated Eye Hospital and Fourth School of Clinical Medicine, Nanjing Medical University, Nanjing, China
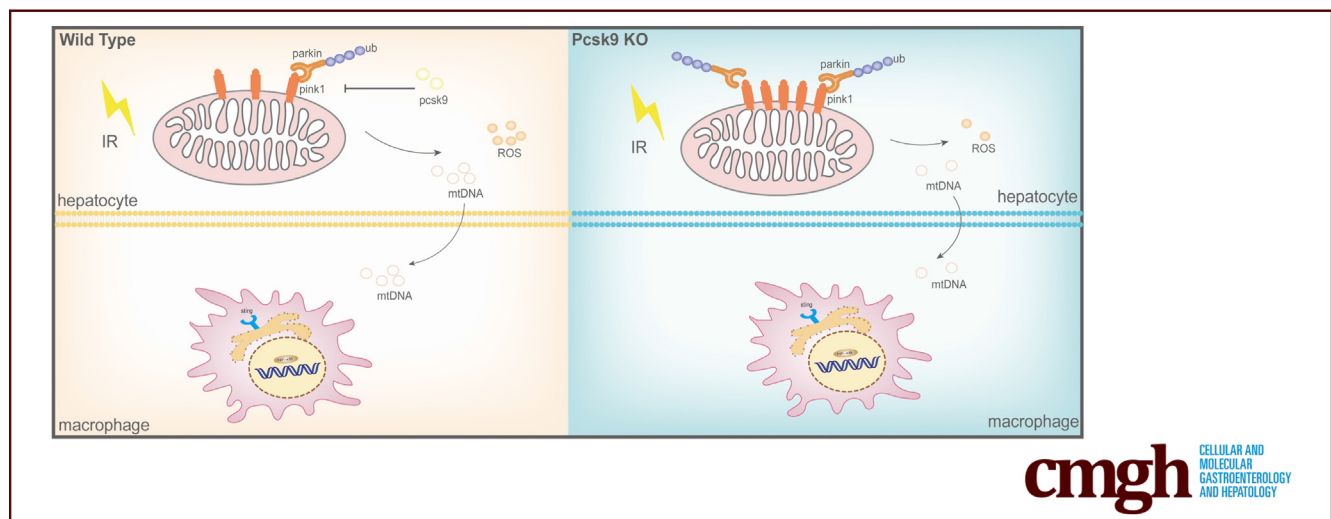
SUMMARY

PCSK9 is up-regulated in response to ischemia-reperfusion injury and plays a significant role in hepatic ischemia-reperfusion injury. This study reveals that hepatocyte PCSK9 inhibits PINK1-Parkin–mediated mitophagy, leading to the activation of STING/NRLP3-induced inflammatory responses, which exacerbate hepatic ischemia-reperfusion injury.

BACKGROUND & AIMS: Hepatic ischemia-reperfusion injury is a significant complication of partial hepatic resection and liver transplantation, impacting the prognosis of patients undergoing liver surgery. The protein proprotein convertase subtilisin/kexin type 9 (PCSK9) is primarily synthesized by hepatocytes and has been implicated in myocardial ischemic diseases. However, the role of PCSK9 in hepatic ischemia-reperfusion injury remains unclear. This study aims to investigate the role and mechanism of PCSK9 in hepatic ischemia-reperfusion injury.

METHODS: We first examined the expression of PCSK9 in mouse warm ischemia-reperfusion models and AML12 cells subjected to hypoxia/reoxygenation. Subsequently, we explored the impact of PCSK9 on liver ischemia-reperfusion injury by assessing mitochondrial damage and the resulting inflammatory response.

RESULTS: Our findings reveal that PCSK9 is up-regulated in response to ischemia-reperfusion injury and exacerbates hepatic ischemia-reperfusion injury. Blocking PCSK9 can alleviate hepatocyte mitochondrial damage and the consequent inflammatory response mediated by ischemia-reperfusion. Mechanistically, this protective effect is dependent on mitophagy.

CONCLUSIONS: Inhibiting PCSK9 in hepatocytes attenuates the inflammatory responses triggered by reactive oxygen species and mitochondrial DNA by promoting PINK1-Parkin–mediated mitophagy. This, in turn, ameliorates hepatic ischemia-reperfusion injury. *(Cell Mol Gastroenterol Hepatol 2024; 17:149–169; https://doi.org/10.1016/j.jcmgh.2023.09.004)*

Because of the rich blood supply to the liver, temporary occlusion of liver blood flow is commonly used to control intraoperative bleeding in liver surgery. However, this procedure leads to unavoidable ischemia-reperfusion injury (IRI).[1] The global rise in nonalcoholic fatty liver disease, diabetes mellitus, and an aging population has made pathologic or marginal livers more susceptible to IRI during surgery.[2–4] Given this scenario, it remains crucial to investigate the mechanisms underlying hepatic IRI.

Proprotein convertase subtilisin kexin 9 (PCSK9) is a secreted protein that promotes the degradation of low-density lipoprotein receptors, resulting in increased serum low-density lipoprotein cholesterol levels.[5] Previous research on PCSK9 has mainly focused on atherosclerosis and subsequent myocardial infarction.[6] However, the role of PCSK9 beyond the cardiovascular system has recently gained attention, including its involvement in renal IRI[7] and stroke.[8] Nevertheless, the function of PCSK9 in hepatic IRI remains unknown.

Aseptic inflammation activation is a crucial pathophysiological process in hepatic IRI.[9–11] Numerous studies have revealed that the cascade of inflammatory signals released in response to injury involves the intrinsic regulatory role of PCSK9. For instance, PCSK9 promotes infiltration of Ly6C^{hi} monocyte-derived macrophages and expression of inflammatory cytokines in the aortic vessel walls of atherosclerotic mice.[12] Conversely, inflammatory mediators can stimulate PCSK9 secretion through toll-like receptors,[13] NOD-like receptor (NLR) family pyrin domain-containing 3 (NLRP3) inflammasomes,[14] and nuclear factor kappa B (NFκB),[15] resulting in inflammation-induced positive feedback. Hence, the interplay between PCSK9 and inflammatory cytokines may be significant in hepatic IRI.

Hepatocyte mitochondrial damage is a crucial component of hepatic IRI and is closely associated with ongoing inflammation. During reperfusion, the sudden restoration of oxygen leads to the generation of reactive oxygen species (ROS), which can harm the mitochondrial membrane and mitochondrial DNA (mtDNA) in hepatocytes when produced excessively.[16] Conversely, ROS and mtDNA activate NLRP3 inflammasomes and cyclic GMP-AMP synthase (cGAS), respectively, both of which have been implicated in liver IRI.[17,18] After mitochondrial damage, damaged mitochondria are degraded through pentaerythritol tetranitrate–induced kinase 1 (PINK1)-Parkin RBR E3 ubiquitin-protein ligase (Parkin)–mediated mitophagy, which has been reported to alleviate hepatic IRI.[19]

In our study, we observed that deletion of PCSK9 enhanced the recruitment of Parkin to mitochondria through PINK1, thereby promoting mitophagy. This process alleviated mtDNA release and the subsequent activation of cGAS-stimulator of interferon genes (STING)/NLRP3–mediated inflammatory responses, ultimately ameliorating hepatic IRI.

Results

PCSK9 Is Up-regulated in Response to Hepatic Ischemia-Reperfusion

To investigate the involvement and role of PCSK9 in hepatic IRI, we established both an in vivo mouse model and an in vitro AML12 H/R model (Figure 1A). In the in vitro model, we observed that PCSK9 expression was up-regulated in response to hypoxia/reoxygenation (H/R), with the highest expression observed at 12 hours of reoxygenation (Figure 1B). Thus, we adopted a study protocol of 12 hours of hypoxia followed by 12 hours of reperfusion for all subsequent in vitro experiments. Previous studies have indicated that PCSK9, activated in response to inflammatory signaling, is primarily produced by hepatocytes.[20,21] To confirm this, we isolated hepatocytes and nonparenchymal cells from mouse livers that underwent 6 hours of reperfusion using differential centrifugation. Our analysis revealed that PCSK9 expression was predominantly observed in hepatocytes (Figure 1C). Furthermore, we assessed the expression of PCSK9 in hepatocytes at different reperfusion times and found that PCSK9 was up-regulated in the early stages of reperfusion (3 hours, 6 hours), returning to normal levels at 12 hours (Figure 1D). Immunohistochemistry (Figure 1E and F) and immunofluorescence (Figure 1G and H) results confirmed the up-regulation of PCSK9 after IR, with PCSK9 co-localizing with the hepatocyte marker HNF4α. In addition, we collected 12 surgical specimens from patients undergoing partial hepatectomy and observed up-regulation of PCSK9 after IR, as demonstrated by polymerase chain reaction (Figure 1I) and immunohistochemical analysis (Figure 1J and K).

PCSK9-/- Ameliorates Liver Ischemia-Reperfusion Injury

Further investigation into the role of hepatocyte PCSK9 in hepatic IRI revealed a reduction in damage in PCSK9-/- mice. Both wild-type (WT) and knockout (KO) groups underwent 90 minutes of ischemia, followed by 6 hours of reperfusion. Tissue damage was assessed using H&E

staining (Figure 2A), and the tissue damage Suzuki score was significantly lower in the KO group (Figure 2B). Serum hepatic transaminases (Figure 2C and D) and the inflammatory cytokines interleukin (IL) 1β, tumor necrosis factor alpha (TNFα), and monocyte chemotactic protein-1 (MCP1) (Figure 2E) were also lower in the KO group compared with the WT group. In addition, the expression of inflammatory cytokine mRNAs in liver tissue was reduced in the KO group (Figure 2F). Neutrophil activation and recruitment play a crucial role in the inflammatory response to hepatic IR. Evaluation of chemokine expression and neutrophil infiltration in the liver revealed down-regulation of chemokines in the KO group (Figure 2G) and a decrease in the number of ly6G+ neutrophils infiltrating the liver (Figure 2H and I).

Hepatocytes undergo apoptosis due to acute hypoxia during hepatic ischemia, which impairs liver function. Our investigation demonstrated that PCSK9-/- reduced hepatocyte apoptosis induced by IR (Figure 3A). The number of terminal deoxynucleotidyl transferase dUTP nick-end labeling (TUNEL) staining-positive cells was significantly lower in the KO group compared with the WT group (Figure 3B). To study the inhibitory effect of R-IMPP, a novel antisecretory small molecule that binds to 80s ribosomes and prevents PCSK9 post-transcriptional translation, in vitro tests were conducted.[22] The effectiveness of R-IMPP's inhibitory effect was confirmed by treating AML cells with R-IMPP for 24 hours and detecting the expression of PCSK9 through Western blotting (Figure 3C). We found that R-IMPP successfully blocked the expression of PCSK9 at a treatment dose of 30 μmol/L or higher. However, at a concentration of 60 μmol/L, R-IMPP damaged mitochondrial membrane potential (Figure 3D and E). Therefore, 30 μmol/L was chosen as the appropriate treatment concentration. In in vitro experiments, H/R induced early apoptosis in AML12 cells, as indicated by phosphatidylserine exposure outside the plasma membrane (detected by Annexin V) and mitochondrial membrane potential collapse (detected by Mitotracker Red). R-IMPP alleviated H/R-induced apoptosis in AML12 cells (Figure 3F).

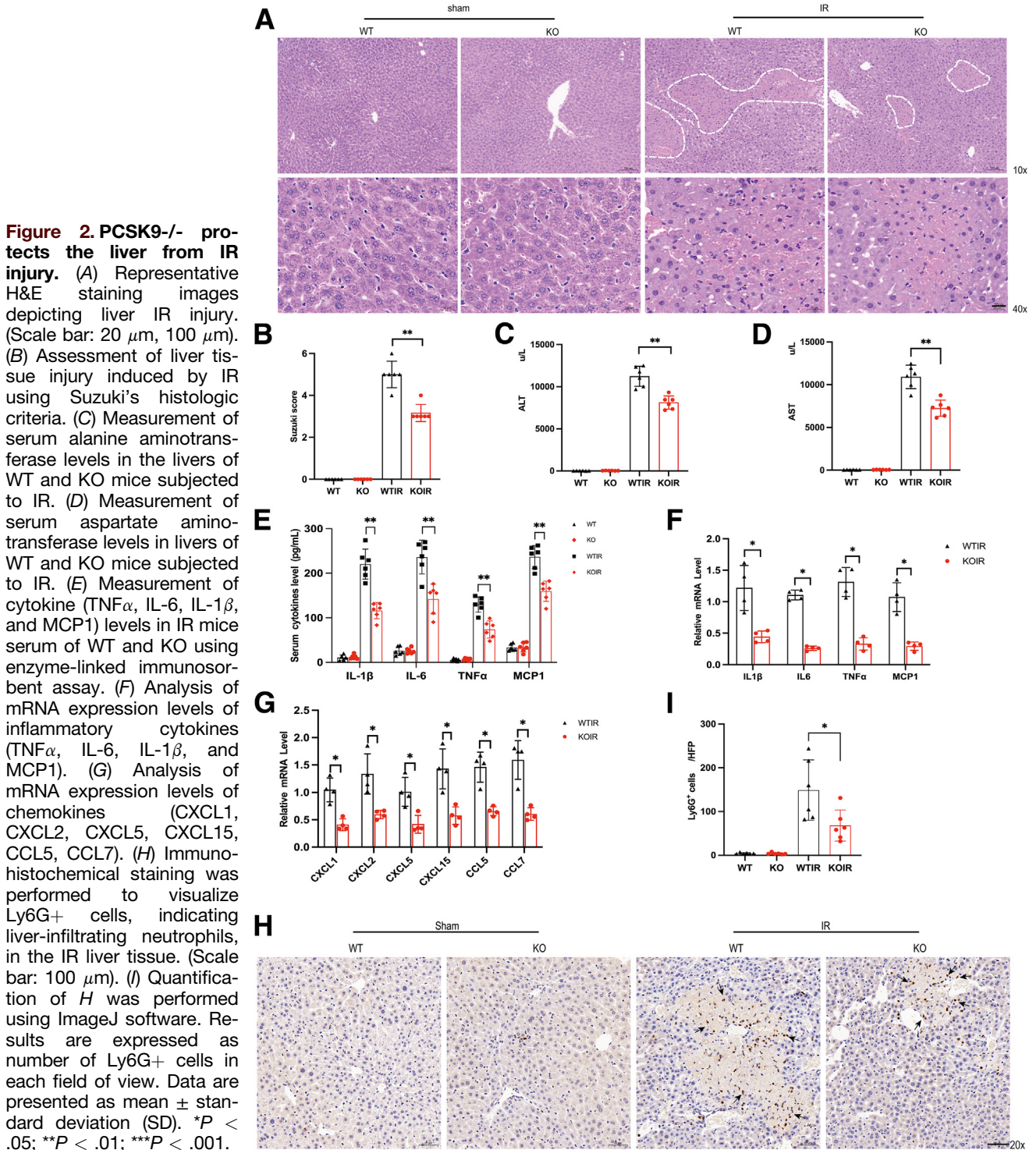## PCSK9-/- Attenuates IR-induced Mitochondrial Damage

Mitochondrial dysfunction and excessive generation of ROS play crucial roles in liver IRI. To assess mitochondrial damage in IR, we examined ROS generation and mitochondrial membrane potential. In the in vivo experiments, liver tissue ROS levels were assessed using dihydroethidium staining of frozen tissue sections (Figure 4A and B). In the in vitro experiments, ROS levels were measured using 2′,7′-dichlorofluorescin diacetate (Figure 4C), and mitochondrial membrane potential was assessed using JC-1 staining (Figure 4D and E). Flow cytometry was used for quantitative analysis of ROS (Figure 4F) and JC-1 (Figure 4G). Consistently, both the in vivo and in vitro results demonstrated that IR and H/R induced ROS production and mitochondrial membrane potential collapse in hepatocytes and AML12 cells. Importantly, inhibition of PCSK9 alleviated this damage. Furthermore, mitochondrial morphology was evaluated using Mitotracker Green (Figure 4H). H/R reduced the fluorescence intensity and disrupted the mitochondrial structure in AML12 cells, whereas inhibition of PCSK9 mitigated mitochondrial damage.

PCSK9 Deficiency Alleviates IR-induced mtDNA Damage and Leakage in Hepatocytes

The accumulation of ROS can cause cellular DNA damage. To assess cellular DNA damage, we performed specific primer extension polymerase chain reaction (Figure 5A). In IR mice, mtDNA amplification was impaired, with 57% reduction in amplification rate, whereas the KO group showed only 16% reduction (Figure 5B). In addition, we observed damage in nuclear DNA (Figure 6A and B). The expression of mitochondrial genes (subunits 1 of NADH dehydrogenase of complex I [ND1], subunits 4 of NADH dehydrogenase of complex I [ND4], subunits 6 of NADH dehydrogenase of complex I [ND6], cytochrome B [cytB]) was down-regulated in WT mice compared with the KO group (Figure 5C). Because mtDNA is an important intracellular damage-associated molecular pattern, we investigated whether PCSK9 affects mtDNA leakage from the mitochondria to the cytoplasm. We found that mtDNA leakage, assessed by Dloop/Tert and Non-Numt/β2m ratio, was down-regulated in the WT group (Figure 5D). To visualize mitochondria and DNA localization, we used Mitotracker Red to label mitochondria and PicoGreen (cytoplasm and nucleus) and DAPI (nucleus) to trace double-stranded DNA. The mtDNA was defined as the

Figure 1. (*See previous page*). **Hepatic IR causes increase in PCSK9 expression.** (*A*) Establishment of liver warm IR model and AML12 cell H/R model was conducted. (*B*) AML12 cells were exposed to H/R by subjecting them to 12 hours of hypoxia followed by reoxygenation for 0, 2, 6, 12, and 24 hours. Then, protein levels of PCSK9 were determined by Western blot. (*C*) Hepatic tissues underwent IR (90 minutes of ischemia followed by 6 hours of reperfusion). Hepatocytes and nonparenchymal cells were isolated using differential centrifugation, and protein levels of PCSK9 were determined by Western blot analysis. (*D*) Mice underwent IR with 90 minutes of ischemia followed by reperfusion for 0, 3, 6, 12, and 24 hours. Protein levels of PCSK9 were determined by Western blot analysis. (*E*) Immunofluorescence staining was conducted to visualize the presence of PCSK9 (*red*), HNF4α (*green*), and DAPI (*blue*) in liver tissues of WT and KO mice. (Scale bar: 50 μm). (*F*) Quantification of *E* was performed using ImageJ software. Results were expressed as relative fluorescence intensity of PCSK9/HNF4α. (*G*) Immunohistochemical staining was conducted to visualize the presence of PCSK9 in liver tissues of WT and KO mice. (*H*) Quantification of *G* was performed using ImageJ software. Results were expressed as average optical density. (*I*) mRNA expression levels of PCSK9 were evaluated before hepatic portal blockade and after IR in patients undergoing partial hepatectomy. (*J*) Immunohistochemical staining was performed to visualize expression of PCSK9 before hepatic portal blockade and after IR in patients undergoing partial hepatectomy (scale bar: 50 μm). (*K*) Quantification of *J* was performed using ImageJ software. Results are expressed as mean absorbance. Data are presented as mean ± standard deviation (SD). *P < .05; **P < .01; ****P < .0001.

Figure 2. PCSK9-/- protects the liver from IR injury. (*A*) Representative H&E staining images depicting liver IR injury. (Scale bar: 20 μm, 100 μm). (*B*) Assessment of liver tissue injury induced by IR using Suzuki's histologic criteria. (*C*) Measurement of serum alanine aminotransferase levels in the livers of WT and KO mice subjected to IR. (*D*) Measurement of serum aspartate aminotransferase levels in livers of WT and KO mice subjected to IR. (*E*) Measurement of cytokine (TNFα, IL-6, IL-1β, and MCP1) levels in IR mice serum of WT and KO using enzyme-linked immunosorbent assay. (*F*) Analysis of mRNA expression levels of inflammatory cytokines (TNFα, IL-6, IL-1β, and MCP1). (*G*) Analysis of mRNA expression levels of chemokines (CXCL1, CXCL2, CXCL5, CXCL15, CCL5, CCL7). (*H*) Immunohistochemical staining was performed to visualize Ly6G+ cells, indicating liver-infiltrating neutrophils, in the IR liver tissue. (Scale bar: 100 μm). (*I*) Quantification of *H* was performed using ImageJ software. Results are expressed as number of Ly6G+ cells in each field of view. Data are presented as mean ± standard deviation (SD). *$P < .05$; **$P < .01$; ***$P < .001$.

fraction of co-localization between PicoGreen and Mitotracker Red. Cytoplasmic double-stranded DNA was barely detectable in the control group but increased after H/R and partially co-localized with mitochondria. However, inhibition of PCSK9 significantly reduced this co-localization (Figure 5*E*).

Hepatocyte PCSK9 Inhibits PINK1-Parkin–mediated Mitophagy

When cells experience mitochondrial damage caused by various physicochemical factors, they initiate a mitophagy program to eliminate unhealthy mitochondria and maintain cellular homeostasis.[23] In our experiments, we observed
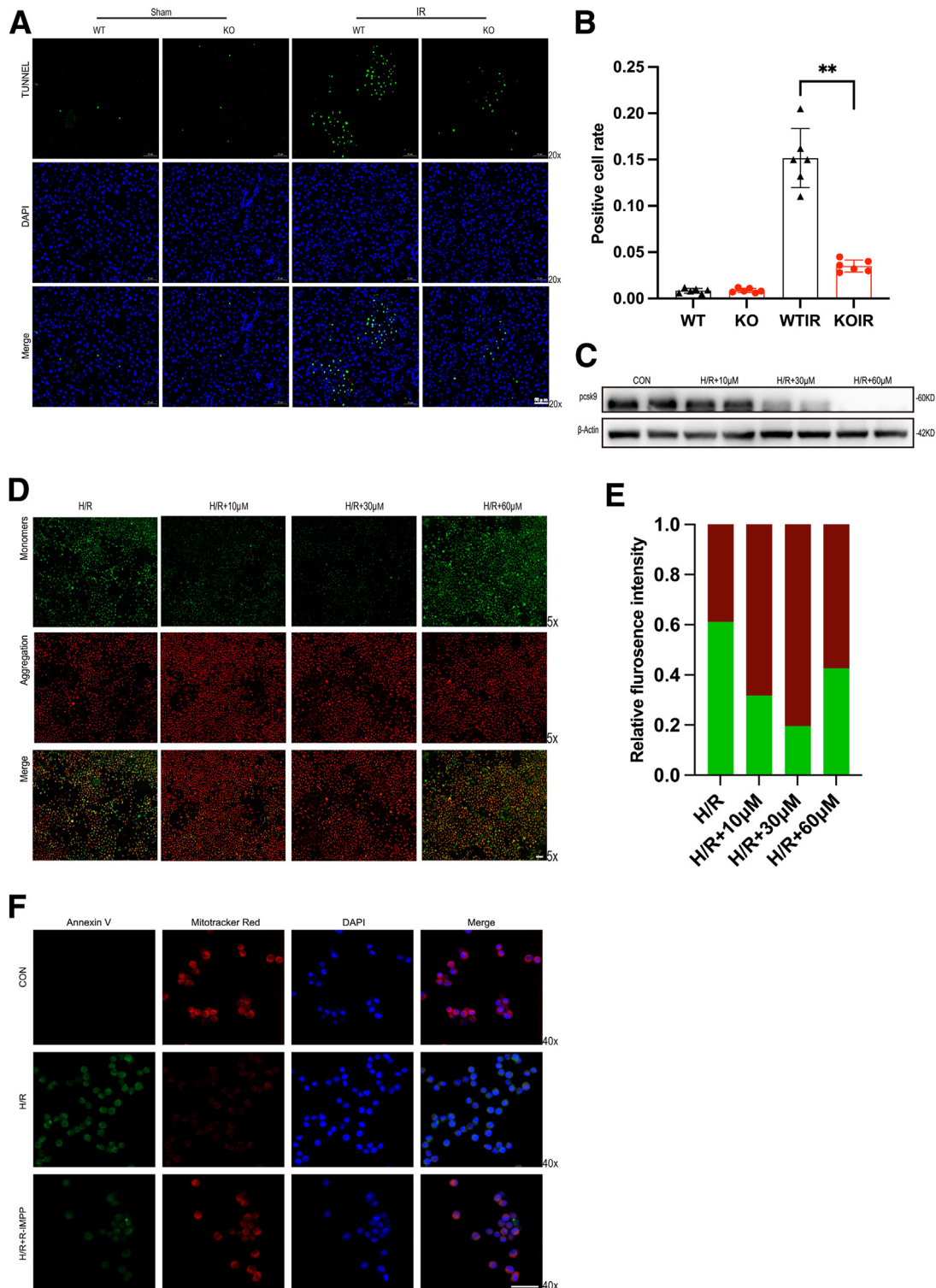
Figure 3. Knockdown of PCSK9 attenuates hepatocyte apoptosis induced by liver IR. (*A*) TUNEL staining of IR liver tissue to analyze apoptosis. (*B*) Quantification of *A*, counted the TUNEL-positive cells and calculated positive cell rate. (*C*) Detected the protein expression of PCSK9 in AML12 cells (treated by R-IMPP for 24 hours with the concentration 10 μmol/L, 30 μmol/L, 60 μmol/L). β-Actin served as loading control. (*D*) JC1 Immunofluorescence staining of AML12 cells (treated by R-IMPP for 24 hours with the concentration 10 μmol/L, 30 μmol/L, 60 μmol/L). AML12 cells were cultured in 6-well plates, and 1$\times$ JC1 was added after R-IMPP stimulation and stained for 30 minutes in 37°C incubator. (*E*) Quantification of *D*, immunofluorescence intensity was detected by Image J. (*F*) Immunofluorescence of H/R AML12 cells to detect Annexin V (*green*), Mitotracker Red (*red*), and DAPI (*blue*). Data represent mean $\pm$ standard deviation. *P < .05; **P < .01; ***P < .001.
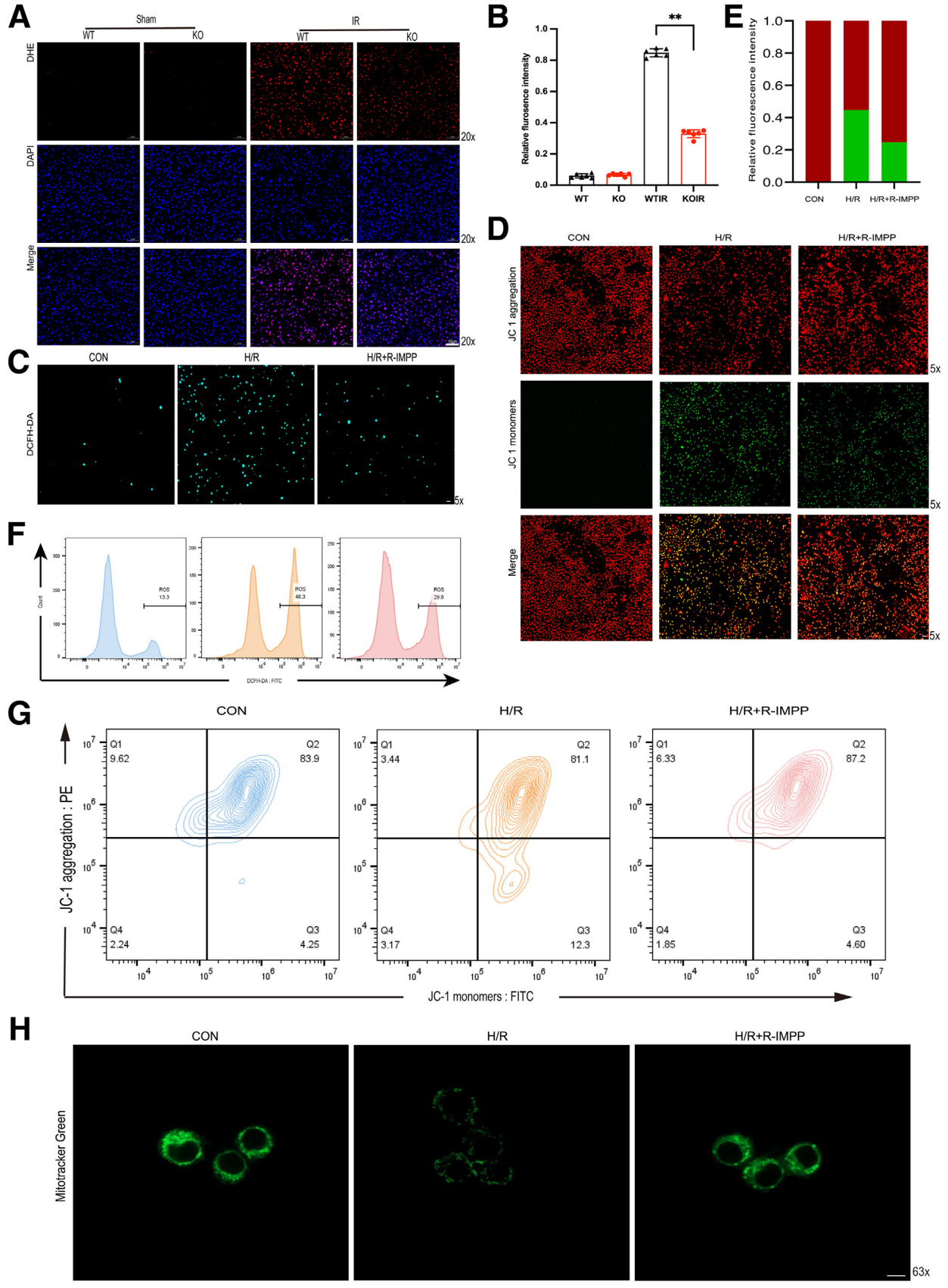
that inhibition of PCSK9 alleviated mitochondrial damage in hepatocytes, both in vivo and in vitro. This led us to question whether PCSK9 inhibition promotes the degradation of damaged mitochondria through the induction of mitophagy. We first examined the immunofluorescence of LC3B and TOMM20 in IR liver tissues and observed co-localization, indicating mitophagy induction in response to IR (Figure 7A). Notably, this effect was more pronounced in the PCSK9 KO group, suggesting that PCSK9 KO enhanced mitophagy. Similar results were obtained in the AML12 cell H/R model (Figure 7B). Previous studies have elucidated the involvement of PINK1-Parkin, BCL2 interacting protein 3 (Bnip3)–BCL2 interacting protein 3 like (Bnip3L), FUN14 domain containing 1 (Fundc1), and FKBP prolyl isomerase 8 (Fkbp8) in initiating the mitophagy program,[24–26] leading us to speculate that PCSK9 may influence mitophagy by modulating the activity of these proteins. We then examined the mRNA expression of these molecules in liver tissue of IR mice using reverse transcription polymerase chain reaction and found that PINK1 and Parkin expression was up-regulated in the KO group, whereas the expression of others remained unchanged (Figure 7C and D). Furthermore, we observed the recruitment of Parkin to the mitochondrial outer membrane in response to H/R (Figure 7E). To assess mitophagy in mitochondria of IR mouse hepatocytes, we conducted Western blot analysis to detect the expression of PINK1, Parkin, TOMM20, and LC3B (Figure 7F and G).

It has been reported that PCSK9 interacts with pentaerythritol tetranitrate (PTEN) and promotes PTEN degradation via the lysosomal pathway.[27] In our study, we confirmed the interaction between PCSK9 and PTEN in AML12 cells (Figure 8A), and inhibition of PCSK9 led to an increase in PTEN expression (Figure 8B). Notably, PINK1 is the putative kinase 1 of PTEN, and PTEN promotes PINK1 expression.[28] To investigate the impact of PTEN activation on mitophagy, we used the PTEN agonist cefminox sodium in the H/R model and observed that PTEN activation enhanced PINK1-Parkin–mediated mitochondrial autophagy (Figure 8C).

In summary, our findings demonstrate that inhibition of PCSK9 promotes PINK1-Parkin–mediated mitochondrial autophagy, and this regulatory effect is mediated through the inhibition of PTEN.

Inhibition of Mitophagy Reverses the Protective Effect of PCSK9 Knockout on Liver IR Injury

To clarify whether PCSK9-/- characteristically alleviates liver IRI through mitophagy, we introduced 3-methyladenine (3-MA) to inhibit mitophagy.[29] Pretreatment with 3-MA before IR and H/R, we found that 3-MA reversed the hepatocyte protective effect of PCSK9 inhibition. H&E staining (Figure 9A) and Suzuki scoring (Figure 9B) revealed liver IRI tissue damage. Reverse transcription polymerase chain reaction measured the expression of inflammatory cytokines (Figure 9C) and chemokines (Figure 9D). TUNEL staining (Figure 9E and F) and Annexin V-mitochondrial staining (Figure 9G) assessed apoptosis in in vivo experiments and in vitro experiments. In addition, we assessed mitochondrial damage with ROS (Figure 10A) and JC1 (Figure 10B and C). Also, mtDNA leakage (Figure 10D) and mtDNA damage (Figure 10E) were detected. The above results showed that 3-MA blockade of mitophagy eliminated the hepatocyte protective effect of PCSK9-/-.

PCSK9-/- Inhibits cGAS-STING Pathway and NLRP3 Activation by Promoting IR Hepatic Mitophagy

In our study, we demonstrated that PCSK9 KO (PCSK9-/-) attenuates the damage to mtDNA induced by liver IRI. Furthermore, in in vitro experiments, inhibition of PCSK9 reduces mtDNA leakage. The cGAS protein acts as a cytoplasmic receptor that recognizes mtDNA and activates STING, leading to the initiation of inflammatory responses.[30] Therefore, we investigated the activation of the cGAS-STING pathway. Our results showed that IR induced the mRNA expression of cGAS, but this up-regulation was suppressed by PCSK9 KO (Figure 11A). Immunohistochemistry (Figure 11B and D) and immunofluorescence (Figure 11C and E) staining of liver tissue further confirmed the expression of phosphorylated STING, which correlated with the changes in cGAS expression. NFκB is a crucial transcription factor involved in inflammation, and its activation promotes the expression of inflammatory cytokines.[31] Previous studies have shown that NFκB acts downstream of STING.[30] Therefore, we examined the protein expression of the cGAS-STING pathway and the phosphorylation of NFκB P65 (Figure 11F and G). PCSK9 deletion down-regulated the expression of cGAS and phosphorylated STING and reduced NFκB P65 phosphorylation. In addition, we observed in the lipopolysaccharide-induced inflammatory response cell model (200 ng/mL, 6 hours) that lipopolysaccharide promotes NFkB P65 nuclear translocation, whereas R-IMPP inhibits this alteration (Figure 11H).

When mitochondria are damaged, mtDNA can leak from the mitochondria to the cytoplasm, and this process can be terminated by mitophagy. We speculated whether PCSK9

Figure 4. (See previous page). PCSK9-/- protects mitochondria from IR-induced damage. (A) Immunofluorescence analysis of ROS using dihydroethidium (DHE) (red) and DAPI (blue) in frozen liver tissues of mice subjected to IR. (Scale bar: 50 μm). (B) Measurement of relative fluorescence intensity of DHE staining. (C) Immunofluorescence detection of ROS in AML12 cells. AML12 cells were cultured in 6-well plates, and 1 mmol/L DCFH-DA was added after H/R and stained for 30 minutes in 37°C incubator. (Scale bar: 200 μm). (D) Immunofluorescence detection of JC1 in AML12 cells. AML12 cells were cultured in 6-well plates and 1× JC1 was added after H/R and stained for 30 minutes in 37°C incubator. (Scale bar: 200 μm). (E) Quantification of Figure 4D was performed using ImageJ software. (F) Measurement of ROS using DCFH-DA in AML12 cells by flow cytometry. (G) Measurement of mitochondrial membrane potential using JC1 in AML12 cells by flow cytometry. (H) Staining of AML12 cell mitochondria using MitoTracker Green. AML12 cells were cultured in confocal dishes with 1 mmol/L Mitotracker and stained for 30 minutes in 37°C incubator. Data are presented as mean ± standard deviation (SD). *$P < .05$; **$P < .01$; ***$P < .001$.
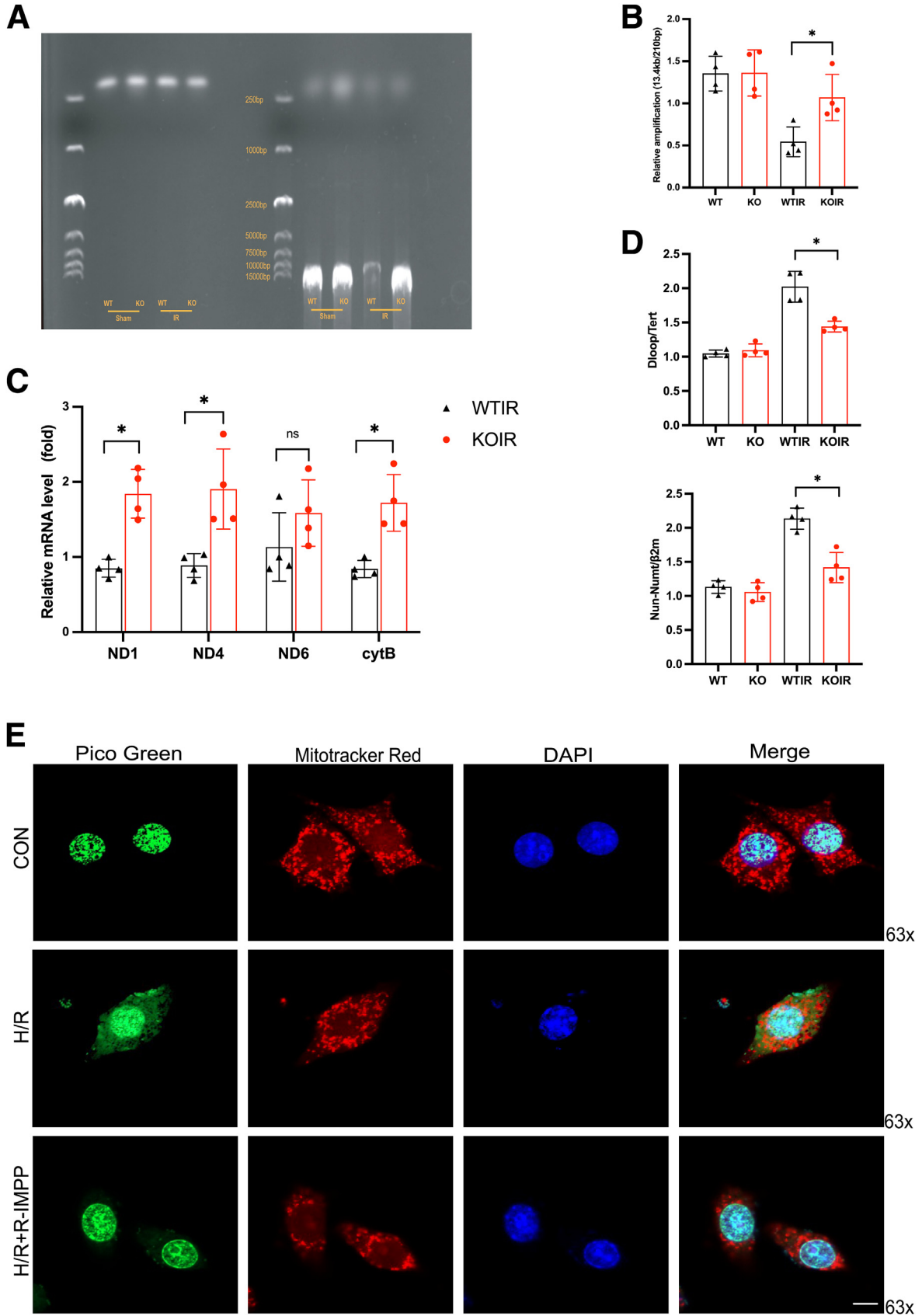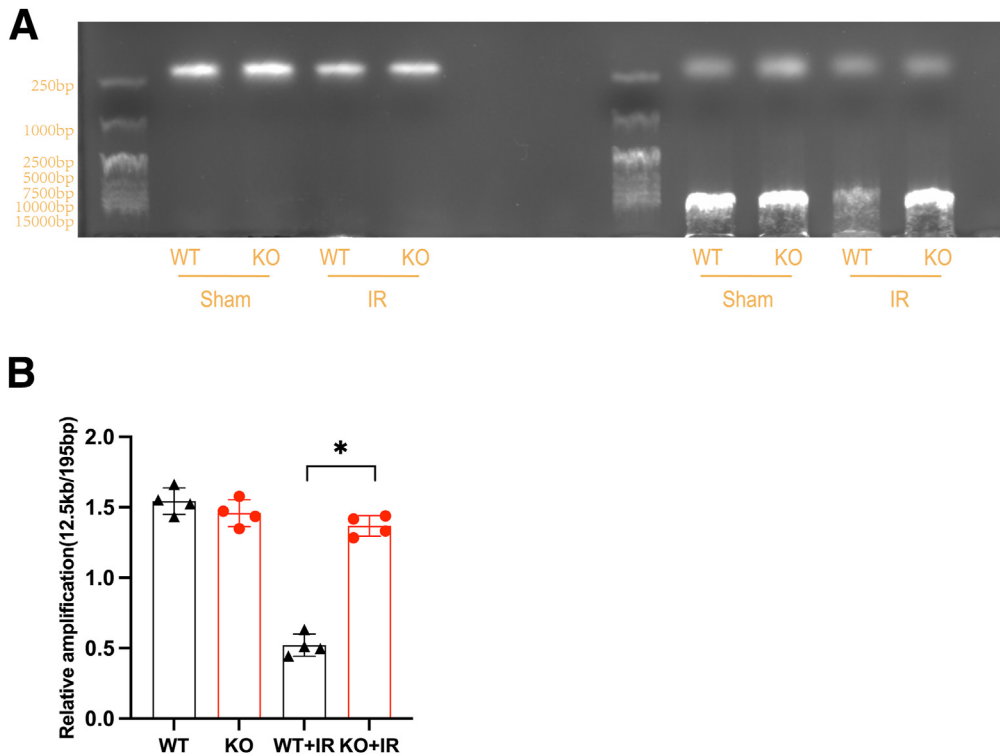
Figure 6. PCSK9 deletion attenuates liver IR-induced nDNA damage in liver tissue. (*A*) nDNA damage (assessed by long and short primers of nDNA) detected by agarose gel electrophoresis. (*B*) Intensity was quantified by ImageJ, and the relative amplification was calculated by normalizing the intensity of the 12.5 kb product to the 195 bp product. Data represent mean ± standard deviation. *$P < .05$; **$P < .01$; ***$P < .001$.

mediates the activation of the cGAS-STING pathway by inhibiting mitophagy. To test this, we pretreated cells with 3-MA (a mitophagy inhibitor) before subjecting them to IR. We found that the down-regulation of STING expression caused by PCSK9 KO could be reversed by 3-MA (Figure 11*I* and *J*). NLRP3 is an important inflammatory complex associated with liver IRI,[18] and STING is involved in the activation of NLRP3.[32] Therefore, we also examined the expression of NLRP3 in liver tissue from IR mice. As expected, NLRP3 expression was up-regulated in the livers subjected to IR. Similarly, the down-regulation of NLRP3 expression caused by PCSK9 deletion was reversed by the inhibition of mitophagy (Figure 12*A* and *B*).

Discussion

The rising life expectancy of the population and the global prevalence of metabolic syndrome have presented new challenges in the field of liver surgery. These challenges stem from 2 primary scenarios. First, individuals with pathologic livers are susceptible to IRI during liver surgery. Second, because of the shortage of suitable donors, marginal donors undergo IRI during liver transplantation. It is evident that these livers undergo more severe damage during the process of ischemia and reperfusion.

Mitochondria serve as energy metabolism factories that are susceptible to malfunction during IR, potentially impacting the recovery of liver function in patients undergoing liver surgery. The disturbance of the tricarboxylic acid cycle and the accumulation of ROS caused by succinate during ischemia are recognized as early contributors to IRI.[33] Excessive ROS and Ca^{2+} overload impact the mitochondrial membrane permeability transition pore during IR, resulting in the persistent opening of the membrane permeability transition pore.[34] This persistent opening of the membrane permeability transition pore leads to the collapse of mitochondrial membrane potential. Mitochondrial damage leads to the release of mitochondrial contents, including mtDNA[35] and cytochrome C,[36] into the cytoplasm. This process activates the cGAS-STING pathway and triggers

Figure 5. (*See previous page*). PCSK9 deficiency reduces IR-induced mtDNA damage and leakage in hepatocyte. (*A*) Long and short fragments of mtDNA were amplified using specific primers by polymerase chain reaction, and mtDNA damage was assessed through agarose gel electrophoresis. (*B*) Quantification of Figure 5*A* was performed using ImageJ software, and the relative amplification was calculated by normalizing the intensity of the 13.4 kb product to that of the 210 bp product. (*C*) Expression levels of mitochondria-related genes (ND1, ND4, ND6, cytB) in WT/KO liver tissues were assessed through mRNA analysis. (*D*) Assessment of mtDNA leakage in WT/KO liver tissues subjected to IR. Results were expressed as the ratio of D-LOOP (mtDNA) to Tert (nDNA) or Nun-NUMT (mtDNA) to β2m (nDNA). (*E*) Immunofluorescence staining of H/R treated AML12 cells (preconditioned with R-IMPP for 24 hours) to visualize double-stranded DNA using Picogreen, mitochondria using MitoTracker Red, and nuclei using DAPI. Data are presented as mean ± standard deviation. *$P < .05$; **$P < .01$; ***$P < .001$.
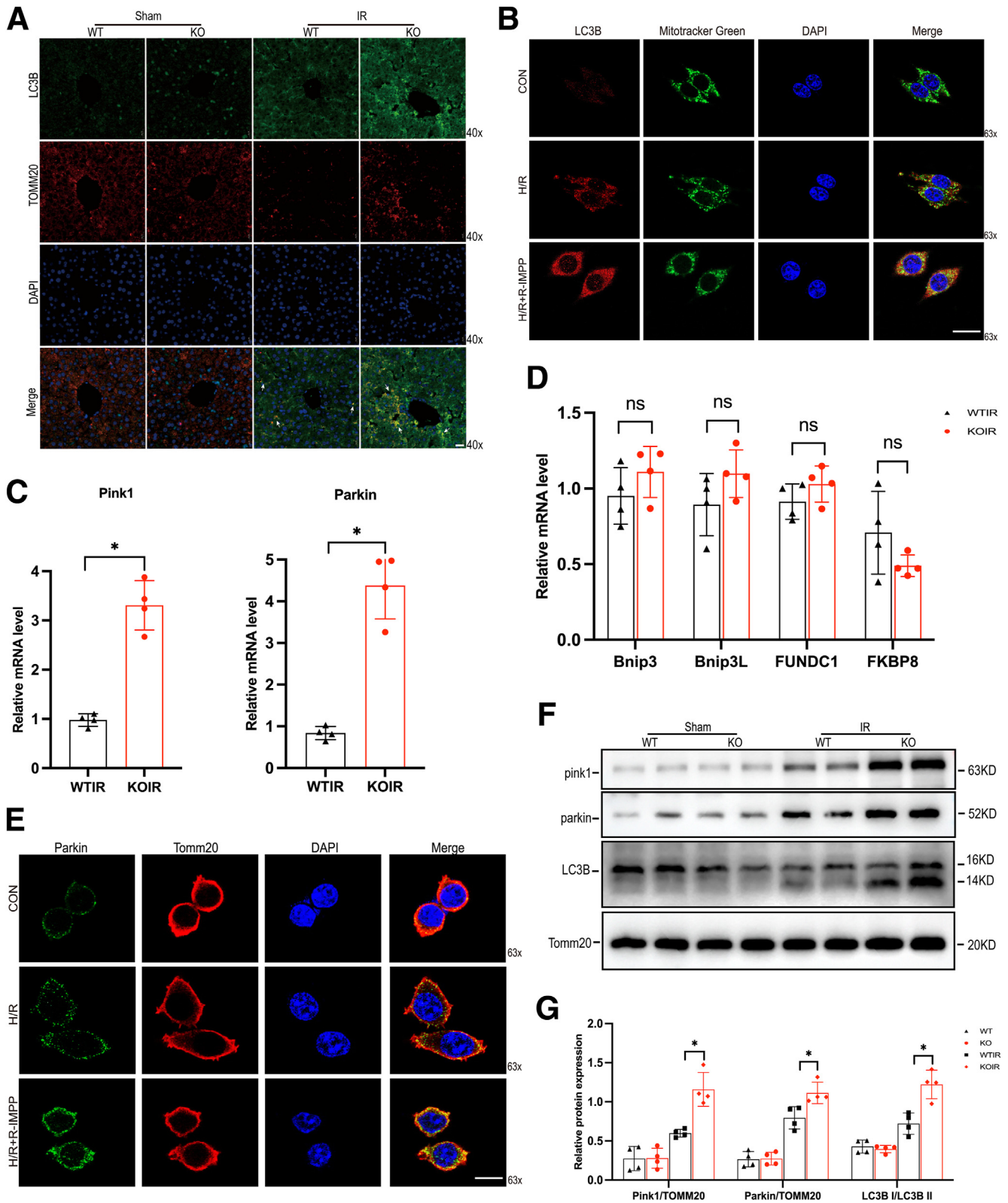
Figure 7. Activation of PINK1-Parkin–induced mitophagy pathways depended on the existence of PCSK9. Representative immunofluorescence images of LC3B (*green*), TOMM20 (*red*), and DAPI (*blue*) in liver tissues of WT/KO mice were captured to visualize autophagosomes, mitochondria, and cell nuclei, respectively (scale bar: 20 μm). (*B*) Representative immunofluorescence images of LC3B (*red*), MitoTracker Green (*green*), and DAPI (*blue*). In treatment group, AML12 cells were pretreated with 30 μmol/L R-IMPP. AML12 cells were incubated at 37° for 30 minutes after H/R modeling using 1 mmol/L Mitotracker working solution. They were then fixed using 4% PFA and incubated with the corresponding primary antibody
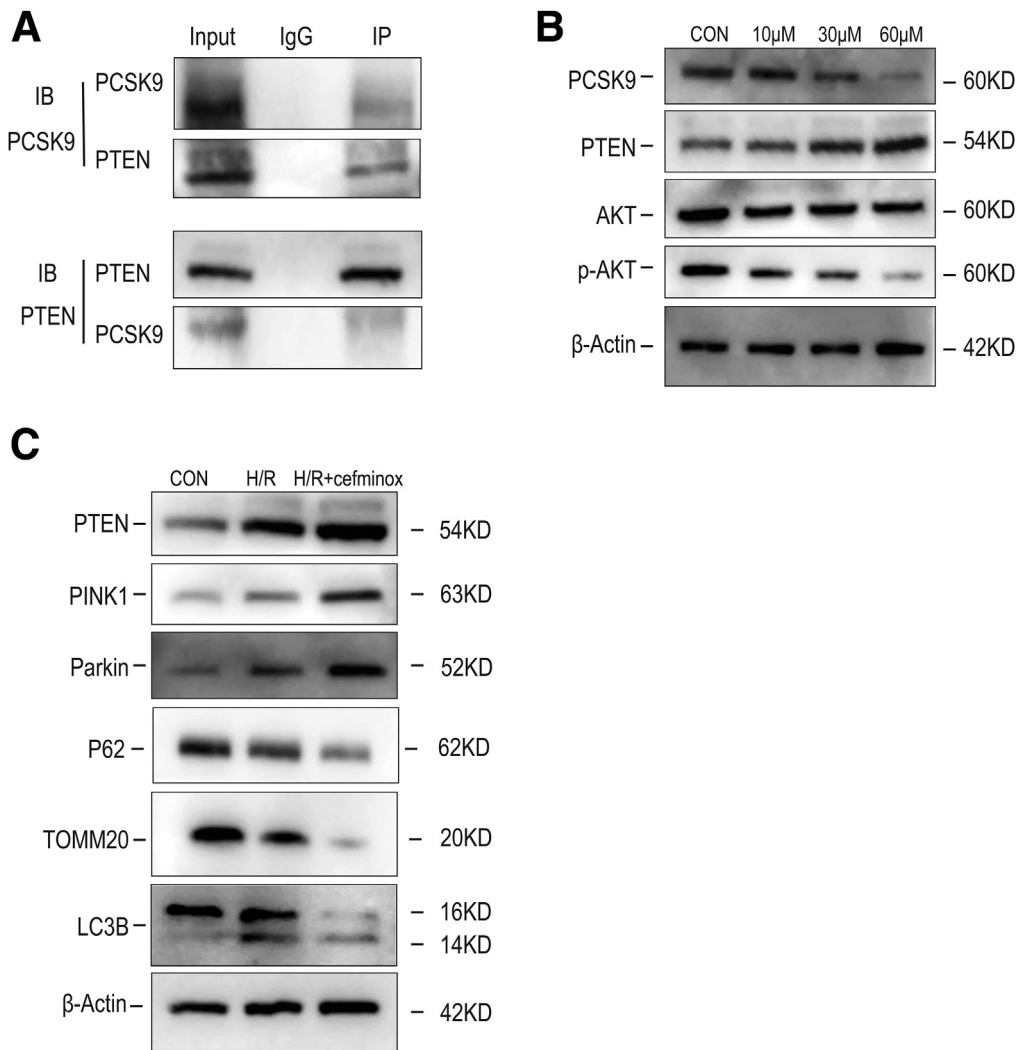
A

B

C

Figure 8. PCSK9 down-regulates PINK1 expression by inhibiting PTEN. (*A*) Western blotting of coIP of PCSK9 and PTEN in AML12 cells. (*B*) Detected PTEN and its downstream (AKT, p-AKT) by Western blot in AML12 cells (treated by PCSK 9, 10 μmol/L, 30 μmol/L, 60 μmol/L). (*C*) Detected mitophagy in H/R AML12 cells (pretreated by cefminox sodium ,10 μmol/L).

endogenous apoptosis. As an important damage-associated molecular pattern, mtDNA plays a significant role in mediating inflammatory responses by activating the cGAS-STING and NLRP3 pathways. Studies have demonstrated that inhibition of mtDNA-cGAS-STING signaling can mitigate hepatic IRI. Prior research has indicated that pre-administration of antioxidants confers protection against IRI in liver tissue of experimental animals.[37] Our investigation involved the measurement of ROS production and mitochondrial membrane potential, which revealed that inhibition of pcsk9 mitigated H/R-induced mitochondrial injury and release of mtDNA.

In fact, PCSK9 has been shown to promote mitochondrial ROS production and induce mtDNA damage in hypoxic cardiomyocytes.[38] In addition, the inhibition of PCSK9 has demonstrated a protective effect on mitochondrial function in rats fed a high-fat diet.[39,40] We also observed a protective effect of PCSK9 inhibition on mitochondrial injury, highlighting the significant role of PCSK9 in mitochondrial dysfunction. However, the underlying mechanism by which PCSK9 exacerbates mitochondrial injury remains unknown.

Mitophagy functions as a protective mechanism by eliminating damaged mitochondria during mitochondrial injury to prevent further damage expansion. PINK1 is a

overnight at 4° in the refrigerator. (*C*) Relative mRNA expression levels of PINK1 and Parkin in liver tissues of WT/KO mice were determined. (*D*) Relative mRNA expression levels of Bnip3, Bnip3L, Fundc1, and FKBP8 were analyzed in liver tissues of WT/KO mice. (*E*) Immunofluorescence staining was performed to visualize the recruitment of Parkin to mitochondria in AML12 cells subjected to H/R. Mitochondria were labeled with Tomm20 (*red*), Parkin was labeled with *green*, and cell nuclei were labeled with DAPI (*blue*). (*F*) Western blot analysis was conducted to detect the expression of mitophagy associated proteins, including PINK1, Parkin, Tomm20, and LC3B, in isolated hepatocyte mitochondria. (*G*) Quantification of the protein expression levels in Figure 7*F* was performed using ImageJ software. Data are presented as mean ± standard deviation. *P < .05; **P < .01; ***P < .001.
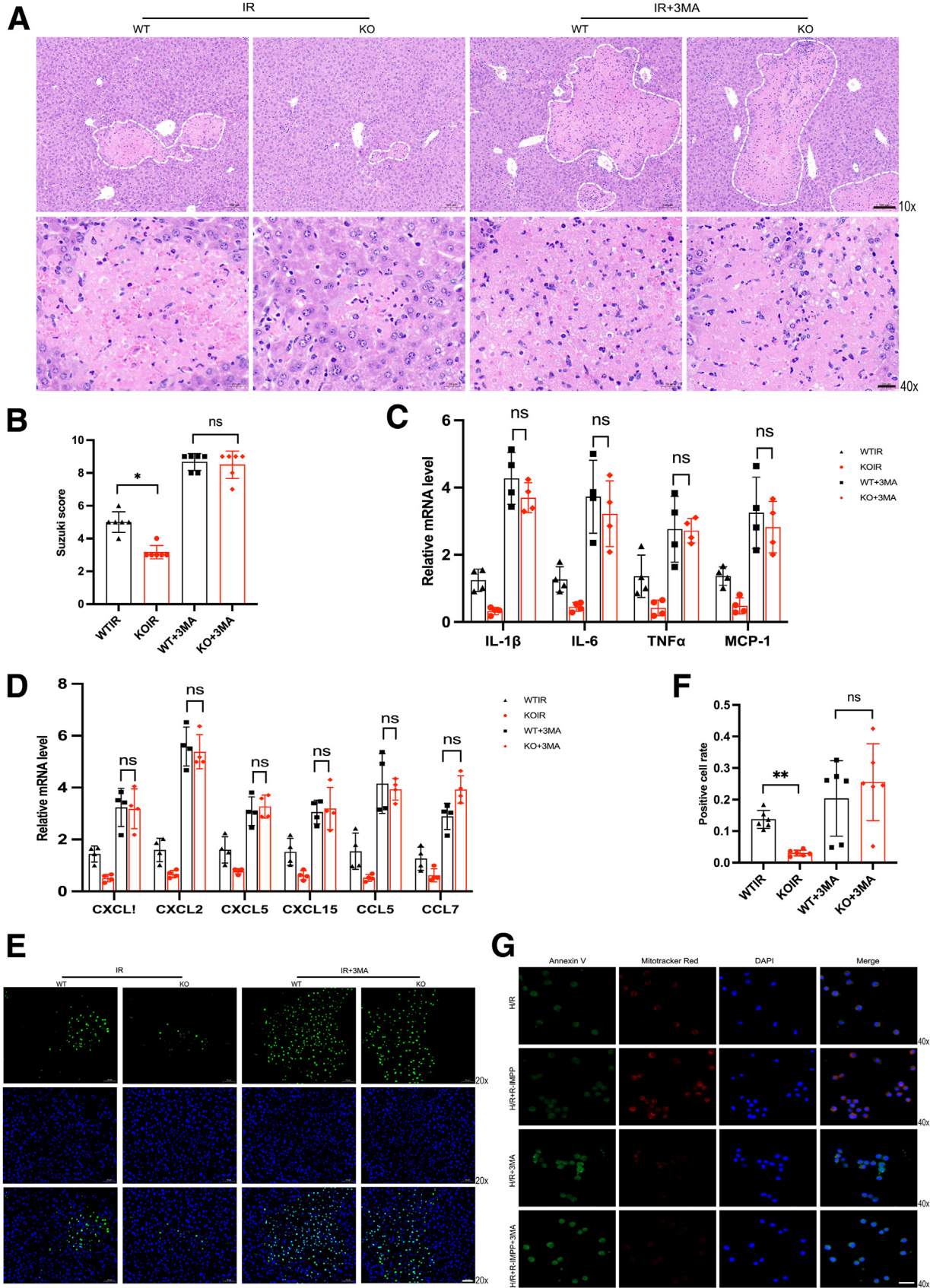
serine/threonine kinase that accumulates in the mitochondrial membrane upon depolarization of the mitochondrial membrane potential. It recruits and activates Parkin, which initiates mitochondrial autophagy by attaching ubiquitin to the mitochondrial membrane through its ubiquitin ligase activity.[41,42] Recent studies have implicated PINK1-Parkin mutations in playing an important role in neurodegenerative pathologies.[43] Interestingly, PCSK9 is highly expressed in patients with Alzheimer's disease,[44,45] and the inhibition of PCSK9 using alirocumab has been found to promote Aβ clearance in animal experiments involving mouse brain tissue.[46] However, no study to date has reported the effect of PCSK9 on the PINK1-Parkin pathway. This has piqued our interest, leading us to speculate that the mitochondrial protective effect of PCSK9 is achieved precisely through the activation of PINK1-Parkin–mediated mitophagy.

To investigate this hypothesis, we explored the role of PCSK9 in the PINK1-Parkin pathway. Our findings revealed that PCSK9 inhibition activated PINK1-Parkin–mediated mitochondrial autophagy. Moreover, we observed that the protective effect resulting from PCSK9 deficiency was reversed upon the inhibition of mitochondrial autophagy using 3-MA. These results suggest the involvement of PCSK9 in the regulation of the PINK1-Parkin pathway.

All in all, our study demonstrated that PCSK9 deletion attenuated liver IRI by promoting PINK1-Parkin–mediated mitophagy, leading to reduced injury in hepatocytes and activation of cGAS-STING/NLRP3–mediated inflammation. However, further research is needed to elucidate the mechanism underlying the interaction between PCSK9 and the PINK1-Parkin pathway.

Methods and Materials
Patient Samples

We collected a total of 12 liver biopsies, including pre- and post-hepatic portal blockade biopsies, from the Hepatobiliary Center of Jiangsu Provincial People's Hospital. Informed consent was obtained from all patients before surgery. The study involving human samples was approved by the Ethics Committee of Jiangsu Provincial People's Hospital (approval number 2023-S RFA-166).

Mouse Warm Ischemia-Reperfusion Model

This study used male C57BL6 WT mice and PCSK9 KO mice. The WT mice were sourced from Vital River Laboratory Animal Technology (Beijing, China), and the PCSK9 KO mice were purchased from Shanghai Southern Model Animal Biotechnology Co. All mice were housed in a specific pathogen-free environment at the Experimental Animal Center of Nanjing Medical University.

For the in vivo experiments, male mice aged 6–8 weeks underwent a fasting period of 8–12 hours before the surgical procedure. Anesthesia was induced using isoflurane, and the arteries and portal veins of the liver's cephalic lobe were clamped using dissection and noninvasive hemostatic forceps, resulting in 70% blockage of blood supply to the liver lobe. After the surgical procedure, the mice were placed on a thermostatic pad set at 37°C to maintain their body temperature.

In the sham-operated group, the blood flow to the liver was not obstructed, serving as the control. The mice were euthanized 6 hours after the reperfusion began, which denotes the restoration of blood supply to the liver lobe.

To inhibit mitophagy in the mouse liver IR model, we used 3-MA (MedChemExpression, HY-19312) administered via intraperitoneal injection at a dosage of 20 mg/kg, given 1 hour before blocking the blood flow in the mice's liver. In the control group, phosphate-buffered saline was administered instead of 3-MA.

The Animal Ethics Committee of the Laboratory Animal Center of Nanjing Medical University (IACUC-2210043) approved all animal experiments conducted in this study, ensuring compliance with ethical guidelines for animal research.

In Vitro Hypoxia/Reoxygenation Model

AML12 cells were cultured in Dulbecco modified Eagle medium supplemented with 10% fetal bovine serum. The H/R model was established following a previously reported procedure.[47] AML12 cells were exposed to hypoxia by placing them in a hypoxia incubator (ThermoScientific STERI-CYCLE i160) with conditions set at 5% CO_2, 1% O_2, and 37°C. After 12 hours of hypoxia, the cells were transferred back to a standard cell culture incubator to restore oxygen supply (reoxygenation).

In the AML12 cells H/R assay, R-IMPP (MedChemExpression, HY-101354) was used to inhibit the expression of PCSK9. The cells were pretreated with R-IMPP at a concentration of 30 μmol/L for 24 hours before the H/R procedure. To enhance the expression of PTEN, AML12 cells were pretreated with cefminox sodium (MedChemExpression, HY-128932). The control group was treated with dimethyl sulfoxide.

Hepatocellular Function Assay

The serum alanine aminotransferase and aspartate aminotransferase levels were measured using the appropriate kits (Servicebio, GM1102, GM1103) to derive the results after an automated biochemical analyzer (Rayto Life and Analytical Sciences Co Ltd Chemray 240).

Figure 9. (*See previous page*). **The protect functions of PCSK9 KO were relied on the mitophagy pathways.** (*A*) H&E staining was performed on WT/KO liver sections to assess liver tissue damage (scale bar: 20 μm, 100 μm). (*B*) Liver injury induced by IR was assessed using Suzuki's histologic criteria. (*C*) mRNA expression levels of cytokines (TNFα, IL-6, IL-1β, and MCP1). (*D*) Chemokines (CXCL1, CXCL2, CXCL5, CXCL15, CCL5, and CCL7) mRNA expression level. (*E*) TUNEL staining was performed on IR liver tissues to assess apoptosis. (*F*) The quantification of Figure 9*E* involved counting the TUNEL-positive cells and calculating the percentage of positive cells. (*G*) Immunofluorescence staining was performed on H/R-treated AML12 cells to detect the presence of Annexin V (*green*), Mitotracker Red (*red*), and DAPI (*blue*). Data are presented as mean ± standard deviation. *P < .05; **P < .01; ***P < .001.

A

B

C

D

E
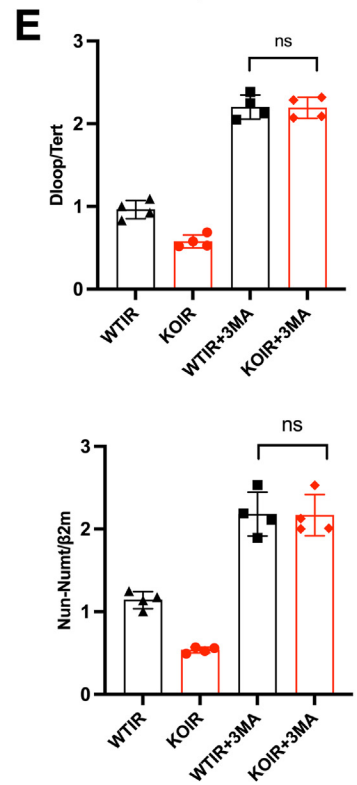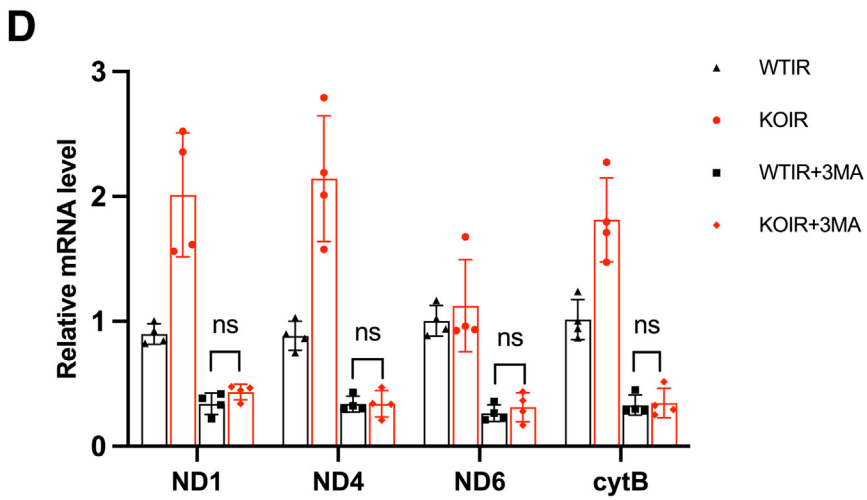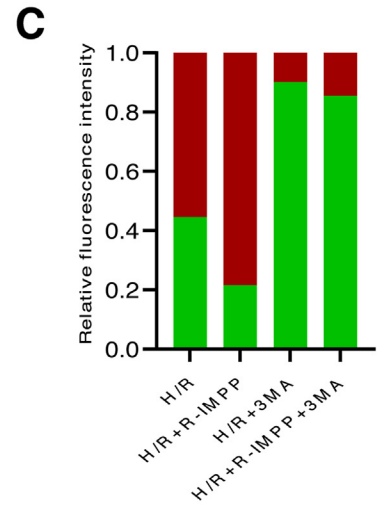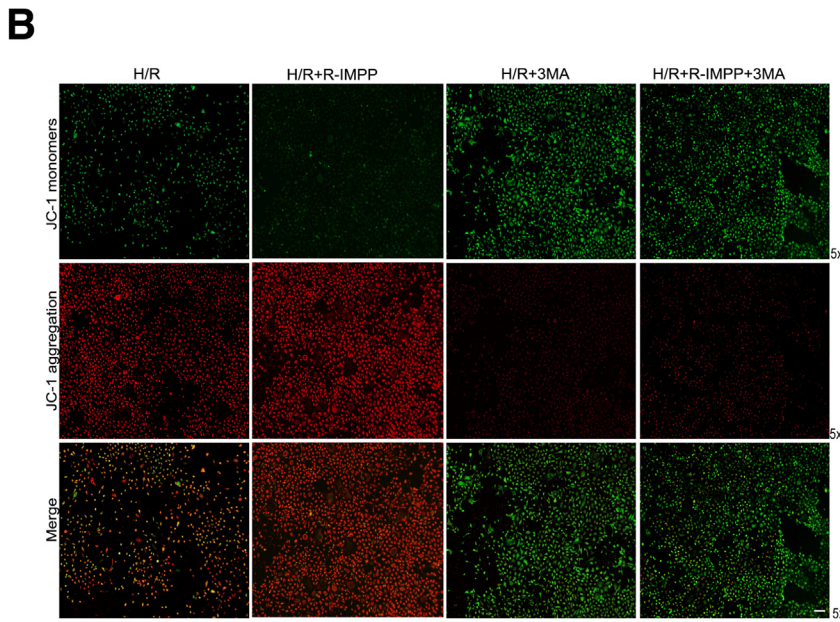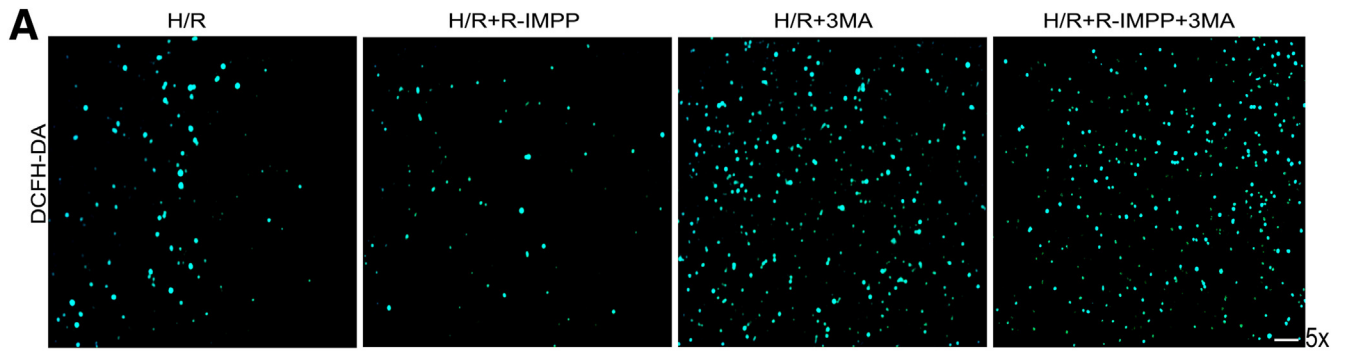
Enzyme-linked Immunosorbent Assay

Mouse serum was collected, and serum IL-1β, IL-6, TNFα, and MCP1 levels were measured using an ELISA kit (Invitrogen, EPX370-40045-901).

Histopathology

The collected liver tissues were soaked in 4% para-formaldehyde (PFA) for 48 hours and then embedded in paraffin. Liver sections were stained with H&E. The severity of liver IR tissue damage was assessed according to Suzuki scoring criteria.

Immunofluorescence and Immunohistochemistry

Liver tissues were soaked in 4% PFA for 48 hours and then embedded in paraffin. After the steps of deparaffinization and antigen repair, the tissue sections were blocked and permeated with 3% bovine serum protein and 0.4% Triton X-100.Then immunohistochemistry and immunofluorescence experiments were performed with the corresponding primary antibodies. After the primary antibody was incubated overnight at 4°C, it was incubated with the appropriate secondary antibody.

Cellular Immunofluorescence

AML12 cells were cultured in confocal dishes (Cellvis, D35C4-20-0-N) and incubated with 1 mmol/L Mitotracker Green for 30 minutes to label mitochondria. Cells were fixed with 4% PFA for 30 minutes, permeabilized using 0.1% Triton X-100 for 2 hours at room temperature and incubated with LC3B primary antibody (Abcam, ab192890) (1:100) overnight at 4°C. Alternatively, cells were incubated with Tomm20 antibody (Abcam, ab186735) and Parkin antibody (Proteintech, 66674-1-lg) (1:100) overnight at 4°C.

RAW264.7 cells were treated with 200 ng/mL lipopolysaccharide for 6 hours, fixed with PFA, permeabilized with Triton X-100, and incubated with p-P65 and p-STING primary antibodies at 4°C overnight.

After H/R, AML12 cells were incubated in medium containing 5% PicoGreen (Thermo Fisher, P11496) and 1 mmol/L Mitotracker Red for 30 minutes at 37°C in a cell incubator following the manufacturer's protocol. Subsequently, the cells were fixed with 4% PFA and stained with DAPI for the nucleus.

Reactive Oxygen and Mitochondrial Membrane Potential Assay

For liver tissue, frozen tissue sections were taken, and liver tissue ROS were assayed using 1 μmol/L dihydroethidium (Servicebio, GDP1018). AML12 cells were

cultured in 6-well plates after H/R stimulation using 1 mmol/L DCFH-DA (Beyotime, S0033M) or 1× JC-1 (Beyotime, C2003S) for 30 minutes at 37°C. Afterwards, reactive oxygen content and mitochondrial membrane potential were measured using fluorescence microscopy or flow cytometry.

mtDNA Damage and Leakage

Total liver tissue DNA was extracted using the QIAamp DNA mini Kit (Qiagen, 172011285), and mitochondrial leakage was measured by real-time reverse transcription polymerase chain reaction. DNA primers were designed to detect Dloop and Non-numt as markers of mitochondrial DNA, Tret and β2m as nuclear DNA, normalizing Dloop to Tert, Non-numt to β2m.[48] The mtDNA damage was amplified by specific mtDNA primers for long and short fragments of mtDNA; after 1 minute at 75°C, polymerase was added, followed by 1 minute at 94°C, cycles of 94°C for 15 seconds, and 65°C for 12 minutes, and a final extension at 72°C for 12 minutes. Mitochondrial DNA and nDNA were amplified with 24 and 28 cycles. The post-polymerase chain reaction products were subjected to agarose gel electrophoresis. The intensity of long fragments was normalized to short fragments to measure relative amplification.

Polymerase Chain Reaction

After extracted from tissues or cells, total RNA (2.0 μg) was reverse-transcribed into cDNA using SuperScript III First-Strand Synthesis System (Invitrogen, Carlsbad, CA). Quantitative polymerase chain reaction was performed using the DNA Engine with Chromo 4 Detector (MJ Research, Waltham, MA). In a final reaction volume of 20 μL, the following were added: 1× SuperMix (Platinum SYBR Green qPCR Kit, Invitrogen, Carlsbad, CA), cDNA, and 0.5 mmol/L of each primer. Amplification conditions were 50°C (2 minutes), 95°C (5 minutes) followed by 50 cycles of 95°C (15 seconds), 60°C (30 seconds). The relative transcript abundance of ND1, ND4 and ND6, respectively, cytochrome B of complex III was quantified by using gene-specific primers (Table 1). The expression levels of chemokines and inflammatory cytokines were also detected by the same method.

Primary Hepatocytes and Nonparenchymal Cells Isolation

Primary hepatocytes and nonparenchymal cells were isolated from mouse livers as we previously described.[49] Briefly, mouse livers were perfused with Hank's balanced salt solution (Gibco, 14170112) containing 0.27% collagenase IV (Sigma, C5318) in the portal vein, after which liver

---

Figure 10.(**See previous page**). **PCSK9-/- attenuates IR-induced mitochondrial damage in hepatocytes.** (*A*) Immunofluorescence staining detected ROS of H/R AML12 cells (pretreated by 3-MA). AML12 cells were cultured in 6-well plates, and 1 mmol/L DCFH-DA was added after H/R and stained for 30 minutes in 37°C incubator. (*B*) Immunofluorescence staining of H/R AML12 cells (pretreated by 3-MA). AML12 cells were cultured in 6-well plates, and 1× JC1 was added after R-IMPP stimulation and stained for 30 minutes in 37°C incubator. (*C*) Quantification of *B*, immunofluorescence intensity was detected by ImageJ. (*D*) mtDNA leakage in WT/KO IR liver (pretreated by 3-MA). Results represented the ratio of D-loop (mtDNA) to Tert (nDNA) or Non-numt (mtDNA) to β2m (nDNA). (*E*) mRNA expression of mitochondrial genes in IR liver (pretreated by 3-MA). Data represent mean ± standard deviation. *$P < .05$; **$P < .01$; ***$P < .001$.
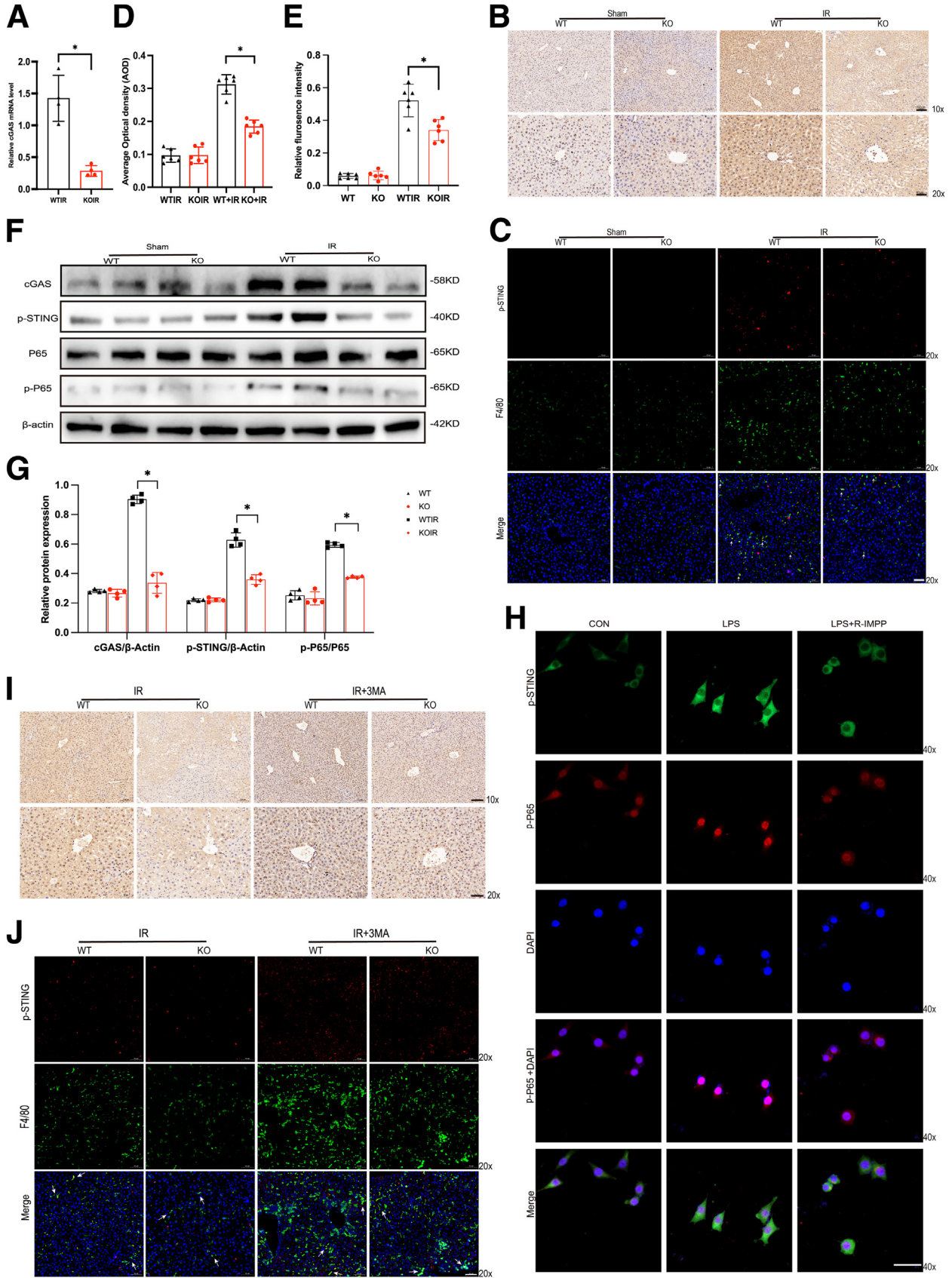
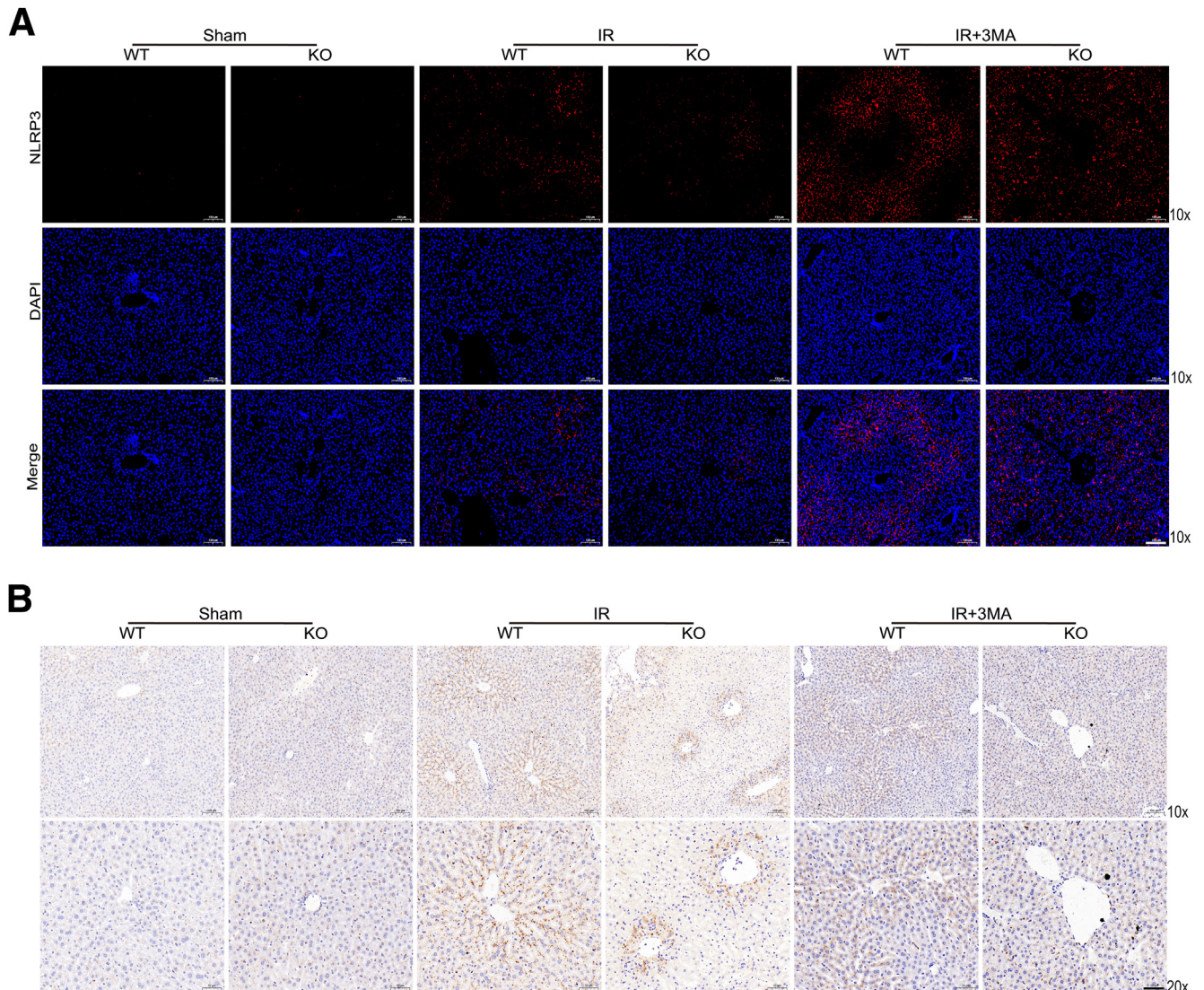**Figure 12. PCSK9-/- inhibits IR-induced activation of NLRP3.** (*A*) Immunofluorescence staining of NLRP3 in mice liver tissue. (*B*) Immunohistochemical staining of NLRP3 in mice liver tissue. Data represent mean ± standard deviation. *$P < .05$; **$P < .01$; ***$P < .001$.

tissue was dissected and teased with forceps, and the cells were filtered through a 70-μm nylon mesh cell filter. Hepatocytes were isolated by centrifugation at 50g for 2 minutes 3 times. The supernatant was collected, and non-parenchymal cells were isolated by centrifugation at 300g for 10 minutes.

Figure 11. (*See previous page*). **PCSK9-/- inhibits mitophagy-associated cGAS-STING activation.** (*A*) The mRNA expression level of cGAS was measured in liver tissues of WT/KO mice. (*B*) Immunohistochemical staining was performed to detect the expression of p-STING in liver tissue of WT/KO mice. (*C*) Immunofluorescence staining was performed to detect the expression of p-STING in macrophages, which were labeled using F4/80. (*D*) Quantification of Figure 11*B* using ImageJ, where the results were expressed as the average optical density. (*E*) Quantification of Figure 11*C* using ImageJ. Results were expressed as the relative fluorescence intensity. (*F*) Western blot analysis was performed to detect the levels of cGAS, p-STING, and the downstream NFκB activation. (*G*) Quantification of Figure 11*F* using ImageJ. (*H*) Raw264.7 cells were treated by lipopolysaccharide (200 ng/mL, 6 hours), and immunofluorescence staining was performed to detect NFκB activation and nuclear translocation in AML12 cells. PCSK9 (*green*), p-P65 (*red*), and DAPI (*blue*). (*I*) Inhibition of mitophagy by pretreatment with 3-MA (20 mg/kg, intraperitoneal injection) before IR, and the expression of p-STING was detected in mouse liver tissues using immunohistochemistry. (*J*) Inhibition of mitophagy by pretreatment with 3-MA (20 mg/kg, intraperitoneal injection), and the expression of p-STING was detected using immunofluorescence.

Table 1. Primers Used in This Study

Gene	Forward primer	Reverse primer
DNA primers		
Dloop	AATCTACCATCCTCCGTGAAACC	TCAGTTTAGCTACCCCCAAGTTTAA
Tert	CTAGCTCATGTGTCAAGACCCTCTT	GCCAGCACGTTTCTCTCGTT
Non-numt	CTAGAAACCCCGAAACCAAA	CCAGCTATCACCAAGCTCGT
β2m	ATGGGAAGCCGAACATACTG	CAGTCTCAGTGGG GGTGAAT
mtDNA long	GCCAGCCTGACCCATAGCCATAATAT	GAGAGATTTTATGGGTGTAATGCGG
mtDNA short	CCCAGCTACTACCATCATTCAAGT	GATGGTTTGGGAGATTGGTTGATGT
nDNA long	TTGAGACTGTGATTGGCAATGCCT	CCTTTAATGCCCATCCCGGACT
nDNA short	AGCCACAGATCCTATTGCCATGC	TGTTGCTTGGTAAACACAGAGGGAAA
RNA primers		
IL-1β	GAAATGCCACCTTTTGACAGTG	TGGATGCTCTCATCAGGACAG
IL-6	CTGCAAGAGACTTCCATCCAG	AGTGGTATAGACAGGTCTGTTGG
TNFα	CAGGCGGTGCCTATGTCTC	CGATCACCCCGAAGTTCAGTAG
MCP-1	GGCTGGAGAGCTACAAGAGG	TCTTGAGCTTGGTGACAAAAAC
CXCL1	CTGGGATTCACCTCAAGAACATC	CAGGGTCAAGGCAAGCCTC
CXCL2	AAAGGCAAGGCTAACTGACCT	CTTTGGTTCTTCCGTTGAGG
CXCL5	AGCTGCGTTGCGTTTGTTTAC	TGGCGAACACTTGCAGATTAC
CXCL15	TTTGTTTGGATCCTGATGCTC	CGGTGGAA0ATTCCTTTTGTT
CCL5	CCAGCAGTCGTCTTTGTCAC	CTCTGGGTTGGCACACACTT
CCL7	CCCTGGGAAGCTGTTATCTTCAA	CTCGACCCACTTCTGATGGG
PINK1	CAGCGAGAGGCCAGCAAGAGAC	CAGGCGATCATCTTGTCCAATTTCA
Parkin	AGGGATTCAGAAGCAGCCAGAGG	CCGGTTTGGAATTAAGACATCG
Bnip3	CAGGGCTCCTGGGTAGAACT	CTACTCCGTCCAGACTCATGC
Bnip3L	CTACCCATGAACAGCAGCAA	ATCTGCCCATCTTCTTGTGG
FUNDC1	AGCGATGACGAATCATACGAAG	CCACCCATTACAATCTGAGTAGC
FKBP8	GAGGACATGGGACAGCCTAC	CCTGGGACCAGTGTCTTCAT
cGAS	GTTCAAACACAAGAAATGCACTG	GCTGACGGAGTACACAATCCT
ND1	TATCTCAACCCTAGCAGAAA	TAACGCGAATGGGCCGGCTG
ND4	TACTAATAATCGCCCACGG	AATTCTCGTGTGTGGGAAGG
ND6	TGGTTGGTTGTCTTGGGTTGGCA	CCGCTACCCAATCCCTCCCT
cytB	GCAACCTTGACCCGATTCTTCGC	TGAACGATTGCTAGGGCCGCG
β-Actin	GGAGATTACTGCCCTGGCTCCTA	GACTCATCGTACTCCTGCTTGCTG

Isolation of Hepatocytes Mitochondria

Mitochondria were extracted from isolated hepatocytes following the reported procedure.[50] Briefly, hepatocytes were homogenized 10 times on ice with 2 mL of Mitochondrial Isolation Reagent (Beyotime, C3601), then the homogenate was centrifuged at $1000g$ for 5 minutes to remove the precipitate, and the supernatant was further centrifuged at $3500g$ for 10 minutes to obtain the mitochondrial precipitate.

Co-Immunoprecipitation

AML12 cells were lysed in NP40 lysate (Beyotime, P0013F) on ice for 30 minutes, and then the lysate was centrifuged at 12,000 rpm for 10 minutes. Primary antibody and protein A+G agarose magnetic beads (Beyotime, P2197S) were added to the supernatant and incubated at 4°C overnight. The next day, the magnetic beads were collected and washed 10 times with NP40. The magnetic beads were added to 1× sodium dodecyl sulfate-polyacrylamide gel electrophoresis loading buffer and boiled for 10 minutes. The collected proteins were then used for Western blot.

Western Blot

Liver tissues were lysed using RIPA to obtain total tissue proteins. After sodium dodecyl sulfate-polyacrylamide gel electrophoresis, they were transferred to polyvinylidene difluoride. For PCSK9 (Abcam, ab185194), p-STING (Invitroen, 35D07A73), cGAS (Abcam, ab252416), NFκB-P65 (Cell Signaling Technology, 6956S), p-P65(Cell Signaling Technology, 3033T), PINK1 (Abcam, ab216144), Parkin (Abceptor, AP6402B), Tomm20 (Abcam, ab186735), P62 (Abcam, ab109012), LC3B (Abcam, ab192890), and β-Actin (Abceptor, AM1021b) antibodies were detected using a chemiluminescence-based method for color development.

Apoptosis Detection

Apoptosis of liver tissue was assessed by TUNEL staining, and the rate of positively stained cells was calculated. Mitochondrial membrane potential and apoptosis detection kit (Beyotime, C1071S) was used to detect apoptosis in H/R-treated AML12 cells, and apoptosis was assessed by observing the mitochondrial membrane potential and the relative fluorescence intensity of Annexin V.

Statistics

Data are expressed as mean ± standard deviation, and statistical differences were determined by GraphPad Prism (San Diego, CA) software. Differences between groups were compared using the non-parametric test Mann-Whitney U test and Kruskal-Wallis test, and $P < .05$ was considered statistically significant.

References

1. Ni M, Zhang J, Sosa R, et al. T-cell immunoglobulin and mucin domain-containing protein-4 is critical for Kupffer cell homeostatic function in the activation and resolution of liver ischemia reperfusion injury. Hepatology 2021; 74:2118–2132.

2. Linecker M, Frick L, Kron P, et al. Exercise improves outcomes of surgery on fatty liver in mice: a novel effect mediated by the AMPK pathway. Ann Surg 2020; 271:347–355.

3. Pratschke S, Arnold H, Zollner A, et al. Results of the TOP study: prospectively randomized multicenter trial of an ex vivo tacrolimus rinse before transplantation in EDC livers. Transplant Direct 2016;2:e76.

4. Pratschke S, Eder M, Heise M, et al. Protocol TOP study (tacrolimus organ perfusion): a prospective randomized multicenter trial to reduce ischemia reperfusion injury in transplantation of marginal liver grafts with an ex vivo tacrolimus perfusion. Transplant Res 2013;2:3.

5. Sabatine MS. PCSK9 inhibitors: clinical evidence and implementation. Nat Rev Cardiol 2019;16:155–165.

6. Qi Z, Hu L, Zhang J, et al. PCSK9 (proprotein convertase subtilisin/kexin 9) enhances platelet activation, thrombosis, and myocardial infarct expansion by binding to platelet CD36. Circulation 2021;143:45–61.

7. Barisione C, Verzola D, Garibaldi S, et al. Renal ischemia/reperfusion early induces myostatin and PCSK9 expression in rat kidneys and HK-2 cells. Int J Mol Sci 2021;22.

8. Rao AS, Lindholm D, Rivas MA, et al. Large-scale phenome-wide association study of PCSK9 variants demonstrates protection against ischemic stroke. Circ Genom Precis Med 2018;11:e002162.

9. Brenner C, Galluzzi L, Kepp O, et al. Decoding cell death signals in liver inflammation. J Hepatol 2013;59:583–594.

10. Huang H, Tohme S, Al-Khafaji AB, et al. Damage-associated molecular pattern-activated neutrophil extracellular trap exacerbates sterile inflammatory liver injury. Hepatology 2015;62:600–614.

11. Zhai Y, Petrowsky H, Hong JC, et al. Ischaemia-reperfusion injury in liver transplantation: from bench to bedside. Nat Rev Gastroenterol Hepatol 2013;10:79–89.

12. Tavori H, Giunzioni I, Predazzi IM, et al. Human PCSK9 promotes hepatic lipogenesis and atherosclerosis development via apoE- and LDLR-mediated mechanisms. Cardiovasc Res 2016;110:268–278.

13. Grune J, Meyborg H, Bezhaeva T, et al. PCSK9 regulates the chemokine receptor CCR2 on monocytes. Biochem Biophys Res Commun 2017;485:312–318.

14. Ding Z, Wang X, Liu S, et al. NLRP3 inflammasome via IL-1beta regulates PCSK9 secretion. Theranostics 2020; 10:7100–7110.

15. Badimon L, Luquero A, Crespo J, et al. PCSK9 and LRP5 in macrophage lipid internalization and inflammation. Cardiovasc Res 2021;117:2054–2068.

16. Zhang H, Yan Q, Wang X, et al. The role of mitochondria in liver ischemia-reperfusion injury: from aspects of mitochondrial oxidative stress, mitochondrial fission, mitochondrial membrane permeable transport pore formation, mitophagy, and mitochondria-related protective measures. Oxid Med Cell Longev 2021; 2021:6670579.

17. Li F, Zhang L, Xue H, et al. SIRT1 alleviates hepatic ischemia-reperfusion injury via the miR-182-mediated XBP1/NLRP3 pathway. Mol Ther Nucleic Acids 2021; 23:1066–1077.

18. Wang Z, Han S, Chen X, et al. Eva1a inhibits NLRP3 activation to reduce liver ischemia-reperfusion injury via inducing autophagy in kupfer cells. Mol Immunol 2021; 132:82–92.

19. Zheng J, Chen L, Lu T, et al. MSCs ameliorate hepato-cellular apoptosis mediated by PINK1-dependent mitophagy in liver ischemia/reperfusion injury through AMPKalpha activation. Cell Death Dis 2020;11:256.

20. Roubtsova A, Munkonda MN, Awan Z, et al. Circulating proprotein convertase subtilisin/kexin 9 (PCSK9) regulates VLDLR protein and triglyceride accumulation in visceral adipose tissue. Arterioscler Thromb Vasc Biol 2011;31:785–791.

21. Seidah NG, Prat A. The multifaceted biology of PCSK9. Endocr Rev 2022;43:558–582.

22. Petersen DN, Hawkins J, Ruangsiriluk W, et al. A small-molecule anti-secretagogue of PCSK9 targets the 80S ribosome to inhibit PCSK9 protein translation. Cell Chem Biol 2016;23:1362–1371.

23. Liu Z, Wang M, Wang X, et al. XBP1 deficiency promotes hepatocyte pyroptosis by impairing mitophagy to activate mtDNA-cGAS-STING signaling in macrophages during acute liver injury. Redox Biol 2022;52: 102305.

24. Ashrafi G, Schwarz TL. The pathways of mitophagy for quality control and clearance of mitochondria. Cell Death Differ 2013;20:31–42.

25. Killackey SA, Philpott DJ, Girardin SE. Mitophagy pathways in health and disease. J Cell Biol 2020;219: e202004029.

26. Teresak P, Lapao A, Subic N, et al. Regulation of PRKN-independent mitophagy. Autophagy 2022;18:24–39.

27. Sun Y, Zhang H, Meng J, et al. S-palmitoylation of PCSK9 induces sorafenib resistance in liver cancer by activating the PI3K/AKT pathway. Cell Rep 2022;40: 111194.

28. Liang H, He S, Yang J, et al. PTENalpha, a PTEN isoform translated through alternative initiation, regulates mitochondrial function and energy metabolism. Cell Metab 2014;19:836–848.

29. Baechler BL, Bloemberg D, Quadrilatero J. Mitophagy regulates mitochondrial network signaling, oxidative stress, and apoptosis during myoblast differentiation. Autophagy 2019;15:1606–1619.

30. Hopfner KP, Hornung V. Molecular mechanisms and cellular functions of cGAS-STING signalling. Nat Rev Mol Cell Biol 2020;21:501–521.

31. Morgan MJ, Liu ZG. Crosstalk of reactive oxygen species and NF-kappaB signaling. Cell Res 2011; 21:103–115.

32. Li N, Zhou H, Wu H, et al. STING-IRF3 contributes to lipopolysaccharide-induced cardiac dysfunction, inflammation, apoptosis and pyroptosis by activating NLRP3. Redox Biol 2019;24:101215.

33. Chouchani ET, Pell VR, Gaude E, et al. Ischaemic accumulation of succinate controls reperfusion injury through mitochondrial ROS. Nature 2014;515:431–435.

34. Seidlmayer LK, Juettner VV, Kettlewell S, et al. Distinct mPTP activation mechanisms in ischaemia-reperfusion: contributions of Ca2+, ROS, pH, and inorganic polyphosphate. Cardiovasc Res 2015;106:237–248.

35. Yu CH, Davidson S, Harapas CR, et al. TDP-43 triggers mitochondrial DNA release via mPTP to activate cGAS/STING in ALS. Cell 2020;183:636–649 e18.

36. Wang Z, Lin D, Zhang L, et al. Penehyclidine hydrochloride prevents anoxia/reoxygenation injury and induces H9c2 cardiomyocyte apoptosis via a mitochondrial pathway. Eur J Pharmacol 2017;797:115–123.

37. Li J, Wang F, Xia Y, et al. Astaxanthin pretreatment attenuates hepatic ischemia reperfusion-induced apoptosis and autophagy via the ROS/MAPK pathway in mice. Mar Drugs 2015;13:3368–3387.

38. Wang X, Li X, Liu S, et al. PCSK9 regulates pyroptosis via mtDNA damage in chronic myocardial ischemia. Basic Res Cardiol 2020;115:66.

39. Amput P, Palee S, Arunsak B, et al. PCSK9 inhibitor effectively attenuates cardiometabolic impairment in obese-insulin resistant rats. Eur J Pharmacol 2020;883:173347.

40. Amput P, Palee S, Arunsak B, et al. PCSK9 inhibitor and atorvastatin reduce cardiac impairment in ovariectomized prediabetic rats via improved mitochondrial function and Ca(2+) regulation. J Cell Mol Med 2020;24:9189–9203.

41. Kane LA, Lazarou M, Fogel AI, et al. PINK1 phosphorylates ubiquitin to activate Parkin E3 ubiquitin ligase activity. J Cell Biol 2014;205:143–153.

42. Nguyen TN, Padman BS, Lazarou M. Deciphering the molecular signals of PINK1/Parkin mitophagy. Trends Cell Biol 2016;26:733–744.

43. Quinn PMJ, Moreira PI, Ambrosio AF, et al. PINK1/PARKIN signalling in neurodegeneration and neuro-inflammation. Acta Neuropathol Commun 2020;8:189.

44. Picard C, Poirier A, Belanger S, et al. Proprotein convertase subtilisin/kexin type 9 (PCSK9) in Alzheimer's disease: a genetic and proteomic multi-cohort study. PLoS One 2019;14:e0220254.

45. Zimetti F, Caffarra P, Ronda N, et al. Increased PCSK9 cerebrospinal fluid concentrations in Alzheimer's disease. J Alzheimers Dis 2017;55:315–320.

46. Mazura AD, Ohler A, Storck SE, et al. PCSK9 acts as a key regulator of Abeta clearance across the blood-brain barrier. Cell Mol Life Sci 2022;79:212.

47. Ge M, Yao W, Yuan D, et al. Brg1-mediated Nrf2/HO-1 pathway activation alleviates hepatic ischemia-reperfusion injury. Cell Death Dis 2017;8:e2841.

48. Zhong Z, Liang S, Sanchez-Lopez E, et al. New mitochondrial DNA synthesis enables NLRP3 inflammasome activation. Nature 2018;560:198–203.

49. Li X, Wang Z, Jiao C, et al. Hepatocyte SGK1 activated by hepatic ischemia-reperfusion promotes the recurrence of liver metastasis via IL-6/STAT3. J Transl Med 2023;21:121.

50. Xu M, Hang H, Huang M, et al. DJ-1 deficiency in hepatocytes improves liver ischemia-reperfusion injury by enhancing mitophagy. Cell Mol Gastroenterol Hepatol 2021;12:567–584.

Correspondence
Address correspondence to: Liyona Pu, PhD, MD, Hepatobiliary Center, The First Affiliated Hospital of Nanjing Medical University, 300 Guangzhou Road, Nanjing, Jiang Su province 210003, China. e-mail: puliyong@njmu.edu.cn; Sheng Han, PhD, Hepatobiliary Center, The First Affiliated Hospital of Nanjing Medical University, 300 Guangzhou Road, Nanjing, Jiang Su province 210003, China. e-mail: hanshengss@163.com; or Yong Ni, MD, PhD, Department of Hepatopancreatobiliary Surgery, Shenzhen Second People's Hospital, The First Affiliated Hospital of Shenzhen University, 3002 Sungang West Road, Shenzhen, China e-mail: niyong123456@163.com.